

VARIABLE SOFT X-RAY EXCESSES IN ACTIVE GALACTIC NUCLEI FROM NONTHERMAL ELECTRON-POSITRON PAIR CASCADES

ANDRZEJ A. ZDZIARSKI¹

N. Copernicus Astronomical Center, Bartycza 18, PL-00-716 Warsaw, Poland

AND

PAOLO S. COPPI²

Department of Astronomy and Astrophysics, University of Chicago, 5640 South Ellis Avenue, Chicago, IL 60637

Received 1990 July 3; accepted 1991 January 31

ABSTRACT

Formation of steep soft X-ray excesses superposed on flatter hard X-ray power-law spectra in nonthermal electron-positron pair cascade sources is studied. Such soft X-ray excesses are similar to those seen below ~ 1 keV in AGN spectra. The soft X-ray excesses in the pair cascade AGN models are due to the Comptonization of UV bump photons by pairs decelerated in the cascade process and thermalized to a nonrelativistic equilibrium temperature. Simple formulae for the spectral form of the excess are found. The soft excess in these models appears as a steep power law superposed on the tail of the UV bump and the flat nonthermal (hard X-ray) power law.

The model parameter space in which an excess is visible in soft X-rays is determined. The excesses typically appear for the hard compactnesses, $10^2 \lesssim l_h \lesssim 10^3$, and for the compactness ratio $1/5 \lesssim l_s/l_h \lesssim 1$. Here $l \equiv L\sigma_T/Rm_e c^3$, the subscripts h and s refer to the luminosities in the X- γ -rays and in the UV photons, respectively, and R is the source size. Taking the UV photons to be a blackbody distribution, a characteristic temperature $kT_s \gtrsim 7$ eV is required for an excess to be visible at 300 eV. Also, the allowed range of l_s/l_h typically increases with the increasing l_h , for l_h up to ~ 300 .

The time variability of soft excesses in pair cascade models is also examined. It is found that the variability patterns of the soft and hard X-rays may be distinctly different (as often seen in AGNs) despite their common origin in the nonthermal source. The form and the amplitude of the soft excesses depend strongly on the luminosity in soft UV photons. The hard X-ray emission, on the other hand, is roughly independent of the UV luminosity. The soft versus hard X-ray variability patterns are classified as a function of the relative variability of the UV luminosity and the power supplied to the relativistic electrons.

Finally, it is found that the parameter space in which soft excesses appear encompasses the range of preferred input parameters for a recently developed Compton reflection model of UV and X-ray emission from the central engine of an AGN. In this model, the observed radiation comes from a nonthermal pair cascade source and a cold ($\sim 10^5$ K), optically thick matter distribution which intercepts and reprocesses part of the nonthermal emission. The presence of soft X-ray excesses in AGNs may thus be understood as a consequence of the presence of both cold matter and nonthermal sources in the central engines of AGNs and additional sources of emission at soft X-ray energies may not be required. In the framework of this model, soft excesses are expected to be anticorrelated with the increasing X- γ -ray luminosity.

Subject headings: galaxies: nuclei — galaxies: X-rays — radiation mechanisms

1. INTRODUCTION

The picture of AGN X-ray spectra that has emerged in recent years is that of a hard X-ray spectrum in the ~ 1 –20 keV range with the canonical average energy spectral index of $\alpha \sim 0.7$ (Rothschild et al. 1983; Turner & Pounds 1989) and a variety of spectra forms below ~ 1 keV (Elvis, Wilkes, & Tananbaum 1985; Wilkes & Elvis 1987; Elvis et al. 1986; Turner & Pounds 1989; Urry et al. 1989). In particular, $\gtrsim 50\%$ – 70% of AGNs exhibit a strong excess of emission above the extrapolation of the hard X-ray power law at energies below ~ 1 keV (Wilkes & Elvis 1987; Turner & Pounds 1989; Urry et al. 1989). Due to poor spectral resolution of both the *Einstein* and *EXOSAT* soft X-ray detectors, the form of the soft excesses has not been well established yet; they have been fitted by either steep power-law, bremsstrahlung, or blackbody

spectra (e.g., Urry et al. 1989). The excesses sometimes extend to 1 keV or more; characteristic energies of the fits to the soft excess spectra in Urry et al. (1989) are from a few tens to a few hundred eV. Hopefully, the spectral form of the excesses will be determined with future data from *ROSAT* and *BBXRT*.

The time variability of the soft excesses exhibits a large variety of patterns. In some cases, the soft excesses and the hard X-rays appear correlated to a certain degree (e.g., Arnaud et al. 1985; Pounds, Turner, & Warwick 1986a). In other cases, the soft excesses vary much more than the hard X-rays (e.g., Piro et al. 1988). For example, declines by factors of 10 and 2 in the soft and hard X-rays, respectively, have been observed in QSO 1821 + 643 (Warwick, Barstow, & Yaqoob 1989). In QSO MR 2251 – 178, the normalizations of both the hard and soft components and the power-law index of the soft component were required to vary in order to fit the variability data (Pan, Steward, & Pounds 1990). In a few cases the soft fluxes remained constant with varying hard X-rays (e.g., Turner &

¹ Work done in part at the Space Telescope Science Institute.

² Work done in part at the California Institute of Technology.

Pounds 1988). Finally, a pivot point at ~ 2 keV has been observed in the variable X-ray spectrum of 3C 120 (Maraschi et al. 1991), implying an anticorrelation of the soft and hard X-ray bands.

The origin of these soft excesses has thus far been a major puzzle in the study of AGNs. As recently reviewed by Begelman (1990), the explanations proposed so far are in doubt as either unlikely to account for the relatively high energies of the excesses (intrinsic radiation of an accretion disk, e.g., Arnaud et al. 1985) or as requiring fine tuning of their parameters (the warm absorber model, e.g., Halpern 1984; Yaqoob, Warwick, & Pounds 1989; Pan et al. 1990).

These explanations, however, have largely ignored another source of “warm” matter that is likely to exist in the interior of AGNs, and that could account for at least part (if not all) of the observed soft excesses. As noted, for example, in Fabian et al. (1986), constraints on the size of the X-ray-emitting region obtained from the rapid X-ray variability observed in many AGNs lead to the conclusion that this region is “compact,” i.e., that it would be optically thick to γ -rays escaping through it. Because AGNs are among the most energetic sources known and γ -rays have been observed to come from them, it is therefore probable that the X-ray-emitting regions contain a sufficient number of electron-positron pairs (produced in the annihilation of γ -rays with lower energy X-rays) to have a Thomson optical depth across the source of order unity. Such a pair plasma could not be ignored as it would reprocess and significantly modify the spectrum of any radiation passing through it. In particular, it could add or subtract a significant amount of luminosity in the range of the soft X-ray excess energies—a complication that *any* model of the soft excess should be prepared to confront.

We will concentrate here on the possibility that the pair plasma is directly responsible for most of the soft X-ray excess. Steep soft X-ray power laws joining onto flatter hard X-ray power laws (qualitatively similar to those seen in observed spectra) have been obtained in nonthermal e^+e^- pair cascade models for some combinations of parameters (Fabian et al. 1986; Svensson 1987, hereafter S87; Lightman & Zdziarski 1987, hereafter LZ87). These models have been proposed to account for the canonical ($\alpha \approx 0.7$) hard X-ray spectra of AGNs. In the models, relativistic pairs with large Lorentz factor are injected within a compact region. The relativistic pairs Compton-upscatter soft photons of the AGN UV bump to X-ray and γ -ray energies. Photon-photon collisions convert some of the γ -rays into secondary e^+e^- pairs, which in turn produce new X-rays and γ -rays. The pairs lose energy and finally thermalize at an equilibrium Compton temperature T_C (typically $kT_C \gtrsim 1$ keV), at which Compton losses of the thermal pairs are balanced by Compton energy gains. The thermal pairs Comptonize the UV photons, which gives rise to a steep power-law spectral component superposed on the flatter (nonthermal) hard X-ray power law. This steep component may well account for the observed soft X-ray excesses.

The idea that AGN soft X-ray excesses may come from nonthermal pair cascade sources has been pointed out in Ghisellini, Done, & Fabian (1989). In general, though, the possibility has received no attention in either the theoretical or observational literature. In this work, we examine the idea in more detail, investigating the constraints on the parameters of the pair cascade sources required for the appearance of excesses, the spectral form of the resulting excesses, and their variability patterns.

What follows will be divided into two main parts. Section 2 focuses on understanding the response of the soft excess to changes in the pair plasma’s energy inputs. Some analytic approximations are given as guides to help visualize the behavior. From these, general constraints on the plasma input parameters are derived such that an observable soft excess be produced by the pair cascade. Section 3 presents numerical calculations of a more realistic model which further illustrate the behavior discussed in § 2. The model is essentially that of Zdziarski et al. (1990b, hereafter Z90) and includes the effect of Compton reflection and reprocessing of X-rays by cold matter located near the pair plasma. We chose this model as it currently appears the most promising in simultaneously accounting for: the canonical average hard (2–10 keV) X-ray spectral index of 0.7, the presence of a $K\alpha$ iron line and the short lag in its response to continuum changes, the hardening of the X-ray spectrum above ~ 10 keV, and constraints from the γ -ray background (see Z90). We note that the allowed parameter space for this model roughly coincides with that for formation of a soft excess. The model may thus also explain why most AGNs appear to show soft X-ray excesses.

2. CONSTRAINTS ON SOFT EXCESSES FROM CASCADE SOURCES

We study here the conditions on the parameters of nonthermal pair cascade sources required for the appearance of observable soft X-ray excesses in their spectra. We will constrain our analysis to pair cascades from monoenergetic (or flat) pair injection, assumed in most pair cascade models of AGNs (e.g., LZ87, S87, Z90). This is the simplest case to understand and has the fewest adjustable parameters. The analysis for more complicated models such as those involving steep injection ($\propto \gamma^{-\Gamma}$, $\Gamma > 2$; e.g., LZ87; Zdziarski, Coppi, & Lamb 1990a, hereafter ZCL90) or pair loading (Done, Ghisellini, & Fabian 1990) is similar and the conclusions drawn here are not significantly affected. In the case of pair loading, for example, the Thomson optical depth for a given set of input parameters is lower and soft excesses consequently appear only at higher rates of energetic pair injection. However, the shape and origin of the excesses are the same as in the case of monoenergetic injection without pair loading. Comparing the results of Done et al. (1990) with those obtained using the numerical codes of LZ87 and Coppi (1991), we have found that the overall parameter space in which soft excesses are visible is the same to within a factor of ~ 2 .

2.1. The Spectral Form of Soft Excesses

The main parameter governing formation of the soft excesses is the thermal Comptonization parameter y (e.g., Rybicki & Lightman 1979). For the model presented here (where the thermal pairs are almost always nonrelativistic), the relevant form of y is given by

$$y = 4\Theta_C \left(\tau_T + \frac{\tau_T^2}{3} \right). \quad (2.1)$$

Here, $\Theta_C \equiv kT_C/m_e c^2$ is the dimensionless Compton temperature, m_e is the electron mass, τ_T is the Thomson optical depth of the thermal pairs, and the factor in parentheses is the average number of scatterings in the source. The y -parameter is determined mainly by the dimensionless compactness

parameters of the nonthermal source:

$$l_h \equiv \frac{L_h \sigma_T}{R m_e c^3}, \quad l_s \equiv \frac{L_s \sigma_T}{R m_e c^3}, \quad (2.2)$$

where L_h , L_s , R , and σ_T are the X- γ -ray luminosity, the part of the UV luminosity that is intercepted by the nonthermal source, the characteristic source size, and the Thomson cross section, respectively. The photon energy up to which the soft excess thermal power law dominates the hard X-ray non-thermal power law depends in turn on the typical energy of the soft photons in the part of the UV bump that is produced close to the nonthermal source. We will approximate the distribution of those UV photons as a blackbody of temperature T_s and corresponding dimensionless temperature $\Theta_s \equiv kT_s/m_e c^2$. The most important of these parameters in a pair cascade source is the compactness l_h .

The optical depth of the thermal pairs, τ_T , is related to l_h and the pair yield Y ,

$$\tau_T = [(4/\pi)Yl_h]^{1/2}. \quad (2.3)$$

The pair yield here is the fraction of the kinetic energy of injected primary pairs that is transformed into rest mass of secondary pairs produced in photon-photon collisions (Guilbert, Fabian, & Rees 1983; S87). At low compactnesses, $l_h \ll 25$, the pair yield Y is much less than 0.1, and consequently τ_T is much less than unity. Thermal Comptonization is effective at such low optical depths only if the pair temperature is relativistic, which occurs only for $l_s \ll l_h$. However, soft excesses do not appear in this case as the amplitude of the blackbody peak does not exceed the amplitude of the power-law spectrum from the nonthermal Compton scattering (see below; ZCL90). Thus, we will consider here only the range of $l_h \gtrsim 25$.

In the absence of thermal Comptonization, a pair cascade spectrum has an approximate power law form. The power law joins at low energies onto the soft photon input spectrum. At high energies, the spectrum steepens gradually, which reflects high-energy breaks in the pair distribution at the maximum energies of pairs from the subsequent pair generations (S87). Above 511 keV, the spectrum also breaks due to the absorption of γ -rays by photon-photon pair production off X-rays.

The optically thick thermal pairs modify this spectrum in three ways. First, the thermal pairs downscatter the hard radiation. This causes a steepening in the spectrum above the break energy,

$$\epsilon_b \simeq 3/\tau_T^2, \quad (2.4)$$

where $\epsilon \equiv E/m_e c^2$ denotes a dimensionless photon energy. At energy $\epsilon \sim \epsilon_b$ the spectral index α increases by 0.5–1 (see Sunyaev & Titarchuk 1980, hereafter ST80; S87). The form of the steepening is independent of the pair Compton temperature, Θ_C , provided $\Theta_C \lesssim \epsilon_b$. Second, the input soft photons are upscattered by the thermal pairs and form a power law tail superposed on the blackbody and the nonthermal power-law spectra. Third, the nonthermal power law is upscattered as well, which results in an increase of its amplitude. The latter two effects strongly depend on the pair temperature, as well as on the optical depth τ_T . We will present a formalism describing their effect on pair cascade spectra below.

The pair yield saturates at very high l_h , reaching the values of $\lesssim 0.2$ (S87; LZ87). In the range of $25 \lesssim l_h \lesssim 1000$, which we will consider here, the pair yield slowly increases with l_h . A fit to an extended set of numerical results obtained using the

method of LZ87 (with inclusion of Coulomb cooling, see ZCL90) is

$$Y \simeq 0.1(l_h/100)^{1/4}, \quad 25 \lesssim l_h \lesssim 1000, \quad (2.5)$$

with an accuracy of $\sim 20\%$. Using this, the optical depth, equation (2.3), becomes

$$\tau_T \simeq 3.6(l_h/100)^{5/8}, \quad 25 \lesssim l_h \lesssim 1000. \quad (2.6)$$

In order to calculate the interior equilibrium Compton temperature (e.g., Krolik, McKee, & Tarter 1981), we will approximate the interior spectrum as a blackbody followed by the nonthermal power law cutoff at ϵ_b . The luminosity in the cutoff power law is taken to be $l_h/2$, which roughly agrees with our numerical results. As we consider here saturated cascades, the index of the nonthermal power law will be $\alpha \simeq 0.9$ –1 (S87). Then, the Compton temperature, Θ_C , becomes,

$$\Theta_C \simeq \frac{\Theta_s l_s + l_c [8 \ln(l_c/5\Theta_s l_h)]^{-1}}{l_s + l_h/2}, \quad l_c \simeq 50; \quad 25 \lesssim l_h \lesssim 1000; \quad (2.7)$$

$$\sim \frac{\text{constant}}{l_s + l_h/2}, \quad \text{for } \Theta_s l_s \ll 1. \quad (2.8)$$

Here, $5\Theta_s$ approximately equals the minimum power law energy; l_c is the compactness at which the cutoff energy $\epsilon_b = 1$; and the pair yield, Y , was assumed here to be a constant related to l_c . (Inclusion of the slow increase of Y with l_h , eq. [2.5], turned out not to improve the accuracy of eq. [2.7].) We have found that $l_c = 50$ provides a good fit to the numerical results in the parameter range of interest here. The maximum deviation of the Compton temperature (2.7) from that found numerically is $\sim 25\%$ for the large number of models we have calculated, which includes those presented in § 3. Note that Θ_C of equation (2.7) decreases slowly with l_h at $l_h \sim l_s = \text{constant}$. The term $\Theta_s l_s$ in the numerator is always negligible for AGNs. When it is negligible, the thermal pairs lose energy in almost all Compton scatterings with the blackbody photon distribution. As the Thomson energy loss rate of an electron is a function of the radiation density only, the Compton temperature is only weakly (logarithmically) dependent on the blackbody temperature.

The Compton parameter, equation (2.1), with τ_T and Θ_C of equations (2.6)–(2.7), differs at most by $\sim 20\%$ from that obtained using the values of τ_T and Θ_C calculated numerically for our set of test cases. We note that for $l_h \gtrsim 25$, when $\tau_T \gtrsim 2$, the term $\tau_T^2/3$ in equation (2.1) dominates. Then, the Compton parameter can be expressed as

$$y \sim \frac{Y \times \text{constant}}{l_s/l_h + 1/2}. \quad (2.9)$$

Substituting the fit of equation (2.5) for Y , we obtain,

$$y \simeq \frac{0.25(l_h/100)^{1/4}}{l_s/l_h + 1/2}, \quad 25 \lesssim l_h \lesssim 1000, \quad (2.10)$$

where the constant gives a good fit to our numerical results. This approximation, in fact, appears to work better than the original one obtained using equations (2.1) and (2.6)–(2.7).

The parameter y is the main parameter governing thermal Comptonization. A narrow initial spectrum acquires a high-

energy power law tail with the index δ ,

$$\delta \simeq \left(\frac{9}{4} + \frac{4}{y} \right)^{1/2} - \frac{3}{2}, \quad (2.11)$$

(Shapiro, Lightman, & Eardley 1976). The thermal spectral index δ has the values 5, 2.4, 1, for y equal to 0.1, 0.3, and 1, respectively. Using equation (16) of ST80, we obtain an approximation for the spectrum from Comptonization of a blackbody spectrum at $\epsilon \lesssim \Theta_C$,

$$\epsilon \frac{dl}{d\epsilon} \Big|_{\text{th,bb}} \approx \frac{15l_s \delta \zeta(\delta+3)}{\pi^4 (2\delta+3)} \left(\frac{\epsilon}{\Theta_s} \right)^{1-\delta} \times \begin{cases} (\delta+3)\gamma(\delta+3, \epsilon/\Theta_s), & \epsilon \gg \Theta_s; \\ \Gamma(\delta+4) & \epsilon \gg (\delta+3)\Theta_s. \end{cases} \quad (2.12)$$

Here γ and Γ are the incomplete gamma function and the gamma function, respectively, and $\zeta(x)$ is the Riemann zeta function. The formula with γ should be used for δ comparable to or larger than ϵ/Θ_s . To compute the value of δ , we use equations (2.10)–(2.11).

The nonthermal power law gets thermally Comptonized as well. A power-law spectrum with the index α beginning at ϵ_a , $(dl/d\epsilon)(\epsilon) = A\epsilon^{-\alpha}$, becomes (using eq. [16] of ST80),

$$\epsilon \frac{dl}{d\epsilon} \Big|_{\text{th,pl}} \approx \frac{A\delta(\delta+3)\epsilon^{1-\alpha}}{\delta(\delta+3) - \alpha(\alpha+3)} - \frac{A\delta(\delta+3)\epsilon_a^{(\delta-\alpha)}\epsilon^{1-\delta}}{(2\delta+3)(\delta-\alpha)}, \quad \epsilon < \Theta_C, \quad (2.13)$$

(the first term above is given in ST80). An example of how well the approximation based on equations (2.12)–(2.13) works is shown in Figure 1.

We see that for $\delta > \alpha$, the original spectral index α is approximately preserved but its normalization increases as shown by the first factor in equation (2.13). This effect may be clearly seen in Figure 1. Equation (2.13) also contains a negative term, which reduces the total spectral component with the thermal index, δ , to a value less than that given by equation (2.12). The normalization constant of the nonthermal power law for saturated pair cascades with $\alpha = 1$ and the compactness $l_h/2$ is

$$A \simeq \frac{l_h}{2 \ln(10/\Theta_s l_h)}, \quad (2.14)$$

consistent with the approximations used for deriving equation (2.7). For $\alpha \neq 1$, the logarithm in the constant A should be replaced by the appropriate power-law integral.

2.2. The Conditions for Observable Soft X-Ray Excesses

We can now narrow down the range of input parameters for which an observationally acceptable soft excess is produced in pair cascade models. The main constraint on the plasma parameters comes from the requirement that the steep thermal power-law component dominate over the flatter nonthermal power law below some threshold energy, E_* . For the purposes of this paper, we will define a soft excess as being “easily observable” below E_* whenever

$$\epsilon \frac{dl}{d\epsilon} \Big|_{\delta} \geq \frac{1}{2} \epsilon \frac{dl}{d\epsilon} \Big|_{\alpha}, \quad \epsilon = \epsilon_*. \quad (2.15)$$

Here $\epsilon_* \equiv E_*/m_e c^2$, the steep power-law component denoted by subscript δ is the sum of equation (2.12) and the second

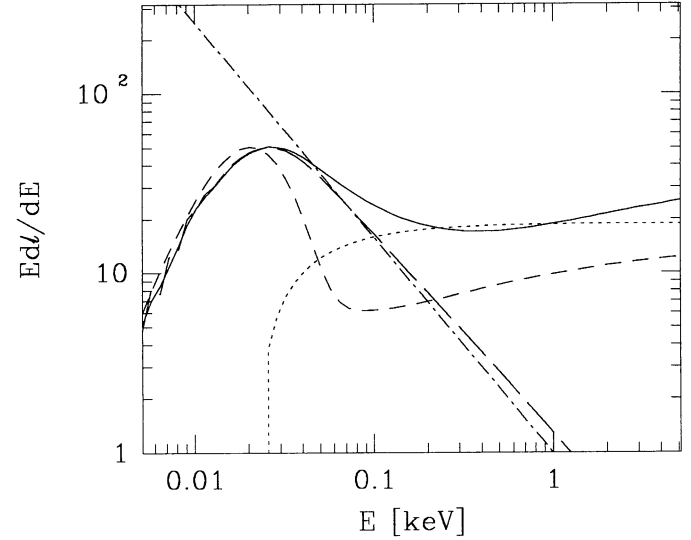


FIG. 1.—Decomposition of spectrum illustrating the effects of thermal Comptonization discussed in § 2. The spectrum was computed using the code of Coppi (1991) and does not include Compton reflection effects. The model assumed monoenergetic pair injection at $\gamma_{\text{max}} = 10^3$ and had input parameters $l_s = 70$, $l_h = 200$, $\Theta_s = 10^{-5}$. The thermal pairs had a numerically computed Thomson optical depth of $\tau_T = 5.52$ and temperature $\Theta_C = 6 \times 10^{-3}$, giving the Compton parameter $y = 0.376$. The solid curve is the total computed spectrum. The long-dashed curve is the contribution of the Comptonized blackbody to that spectrum. The short-dashed curve shows the equilibrium spectrum computed omitting thermal Comptonization (but including the effects of an increased photon escape time due to $\tau_T > 1$), i.e., the underlying un-Comptonized nonthermal power law and blackbody. Note the dramatic amplification of the nonthermal power law by thermal Comptonization. The dot-dashed and dotted curves are respectively the spectra of eqs. (2.12) and (2.13) computed using the approximations of § 2.

(negative) term in equation (2.13), and the nonthermal power-law component denoted by subscript α is the first term in equation (2.13). For l_s or l_h too large, the Compton temperature, Θ_C , can drop below ϵ_* . In that case, the approximations (eqs. [2.12]–[2.13]) used in equation (2.15) become invalid. The thermal power laws rolls over sharply at $\epsilon \sim \Theta_C$ ($< \epsilon_*$) and a soft excess is then not visible at $\epsilon = \epsilon_*$. Hence, we impose an additional condition on the input parameters, namely that

$$\Theta_C \geq \epsilon_*, \quad (2.16)$$

where Θ_C is given by equation (2.7).

Conditions (2.15)–(2.16) define a volume in the three-dimensional parameter space of l_h , T_s , and l_s/l_h in which a visible excess is produced. We can explore the boundaries of this volume by first considering the case where the UV bump temperature, T_s , is fixed. Turning equation (2.15) into an equality one finds that at $E_* \geq 20kT_s$ either one or three values of l_s/l_h satisfy the equality for a given l_h . The largest of these (the root that always exists for $E_* \geq 20kT_s$) corresponds to the point where the UV bump is so prominent that the (slightly Comptonized) blackbody emission at ϵ_* is comparable to the nonthermal power law. The value of this root is only weakly dependent on l_h . For $E_* \geq 20T_s$, this value of l_s/l_h is exponentially large. For $E_* \sim 300$ eV, a typical energy at which excesses are claimed to begin, and realistic T_s (~ 5 – 15 eV), the value is usually too high to possibly correspond to AGNs. If the underlying (un-Comptonized) UV emission is not a

blackbody, the arguments presented here are of course modified. However, as long as the emission rolls over rapidly before reaching soft X-ray energies (e.g., as in most disk models without coronae), an excess due directly to the underlying UV distribution is still unlikely to account for observed excesses.

For $E_* \gtrsim 20kT_s$, the lowest and the middle roots delineate the region of parameter space in which a steep power-law excess is visible. For l_s/l_h greater than the middle root, no excess is visible since the thermal plasma is too cool and thermal Comptonization is negligible. For l_s/l_h less than the lowest root, again no excess is visible as the peak of the blackbody and consequently the thermal power law fall below the nonthermal power law (see Fig. 1). A simple estimate of that value obtained assuming $\alpha = 1$ is

$$\frac{l_s}{l_h} > \frac{3}{2 \ln(10/\Theta_s l_h)} \sim \frac{1}{5}. \quad (2.17)$$

In between the values corresponding to the two roots, a steep power-law excess is observable at $\epsilon \leq \epsilon_*$. In Figure 2, we plot the curves delineating the parameter space corresponding to observable soft excesses over a range of l_h and for several fixed values of T_s . The values of $E_* = 300$ eV and $\alpha = 0.9$ were assumed. The maximum hard compactness in Figure 2, $l_h = 1500$, corresponds approximately to the condition that the break energy ϵ_b of equation (2.4) not fall into the observationally excluded 2–10 keV range. The minimum $l_h = 25$ shown in Figure 2 is the minimum one at which the formalism used here applies.

The lower branches of the curves shown in Figure 2 correspond to the lowest root discussed above. We see that equation (2.17) is indeed a good estimate of that minimum l_s/l_h . The upper branches correspond to the minimum of the middle root of equation (2.15) and the root of the equality in equation (2.16), i.e., $E_* = T_C$. The middle root of equation (2.15) is

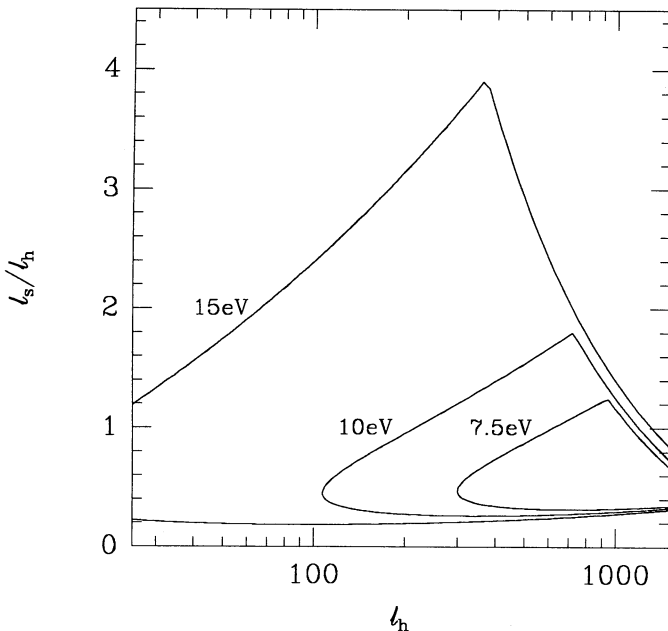


FIG. 2.—The model parameter range $l_h - l_s/l_h$ for which soft X-ray excesses appear. Soft excesses are visible below $E_* = 300$ eV (see eq. [2.15]) for the parameters lying inside the regions enclosed by the solid curves, labeled by the corresponding value of kT_s .

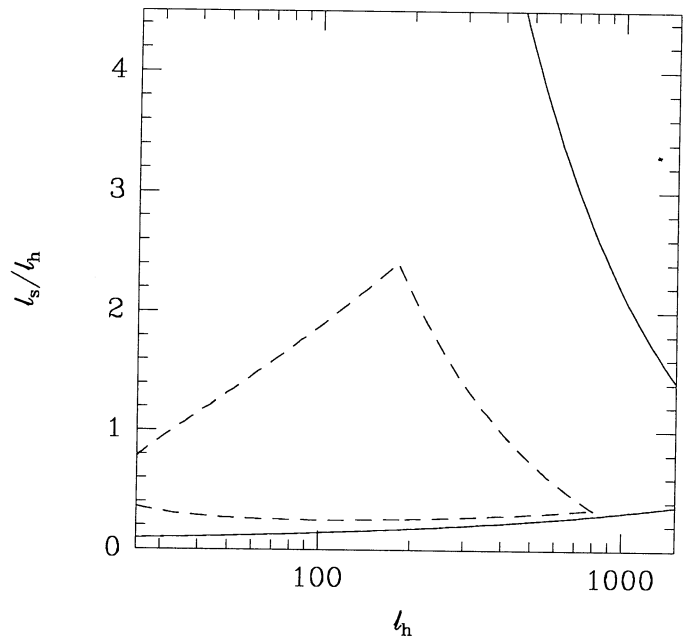


FIG. 3.—The same plot as in Fig. 2 except that $kT_s = 50$ eV, and $E_* = 300$ eV for the solid curve and 1 keV for the dashed curve. An excess visible at 1 keV is in conflict with observations for most AGNs. Models with blackbody temperatures exceeding 50 eV are thus seen as likely to produce too much of an excess at 1 keV and hence are unlikely.

plotted left of the breaks in the upper branches. In the region above the upper branches and to the right of the breaks, the Compton temperature of the thermal plasma is less than E_* , and thus no excess power law is visible in spite of inequality (2.15) being satisfied.

Inspecting the curves in Figure 2, we see that for $l_h \lesssim 10^3$, excesses are visible over a substantial range of parameters when the blackbody temperature kT_s becomes greater than about 7 eV. This range of parameters increases rapidly with increasing kT_s . This effect is mostly due to the origin of the steep power law moving to higher energies, thus increasing the energy at which it intersects the nonthermal power law. By $kT_s = 15$ keV, most of the parameter space shown in Figure 2 gives a visible excess.

If we increase kT_s to such values that $E_* < 20kT_s$, the upper and the middle roots will join and then disappear, and inequality (2.15) will be then satisfied at all values above the one corresponding to the lowest (and now the only) root. At large enough values of kT_s , an excess begins to appear at energies greater than 1 keV, which is not seen observationally in most AGNs. This may be seen in Figure 3 where we show a plot analogous to that of Figure 2 for $kT_s = 50$ eV and $E_* = 300$ eV (solid curves) and 1 keV (dashed curve). The upper solid curve corresponds to $E_* = T_C$. Excesses visible at 300 eV but not at 1 keV occur in the area between the solid and the dashed curves. We see that at $l_s \sim l_h$, which is likely to occur in AGNs (see § 3), excesses appear above 1 keV for most of the range of l_h . Summarizing these considerations, observationally acceptable excesses are possible at $7 \text{ eV} \lesssim kT_s \lesssim 50 \text{ eV}$, with $kT_s \approx 15 \text{ eV}$ corresponding to soft excesses appearing in a large range of the parameter space $l_h - l_s/l_h$.

From Figure 2, we also see that the larger l_h , the wider the range of T_s for which an excess occurs, with weaker effect on the range of l_s/l_h . As the nonthermal index α is an increasing

function of l_h , we predict that AGNs with steeper hard X-ray spectra (and hence larger l_h) should exhibit soft X-ray excesses more often than those with flatter hard X-ray spectra.

Also, as remarked above, the higher T_s , the wider the ranges of l_h and l_s/l_h with soft excesses. If the UV bump is thermal, its temperature increases with decreasing source size (see, e.g., eq. [3.2] below), which is likely to be proportional to luminosity. At a given compactness, we thus predict that low-luminosity AGNs will exhibit soft excesses more often than those with high luminosity.

Finally, we note that $l_s/l_h \sim \frac{1}{2}$ is the value at which a soft excess appears in the largest ranges of T_s and l_h . Thus, AGN models predicting that value of l_s/l_h also indirectly imply the presence of soft excesses, as is the case for the model discussed in § 3 below.

2.3. Time Variability of Soft Excesses

With the above results, we can make some predictions regarding the response of the soft excesses to changes in the plasma input parameters. First, we consider $l_h = \text{constant}$ and decreasing l_s . At $l_s \gg l_h$, the parameter $y \ll 1$, and there is no observable thermal Comptonization. As l_s decreases, the y parameter increases and an increasingly flatter thermal Comptonization tail develops. Note that as y increases, there is an anticorrelation between the soft and hard X-ray fluxes (e.g., see Fig. 7a in § 3). The Comptonization tail originates near the peak of the blackbody and so decreases in overall amplitude as l_s decreases. The normalization of the nonthermal power law, however, increases with decreasing l_s (eq. [2.13]). Thus, at low enough l_s , the power-law tail from thermal Comptonization of blackbody photons disappears again, being negligible compared to the Comptonized nonthermal power law. This behavior can be inferred from Figure 2.

When l_s is constant and l_h increases, the source exhibits a similar behavior. As before, the soft excess power law is negligible at $l_s/l_h \gg 1$ and $\ll 1$, and it is observable in an intermediate interval of l_h . The quantitative differences are that now y increases with decreasing l_s/l_h faster than in the case $l_h = \text{constant}$, l_s decreasing (see eq. [2.10]). Also, the amplitude of the nonthermal power law increases faster than proportional to l_h (eqs. [2.13]–[2.14]). This behavior is illustrated in Figure 4.

When both l_s and l_h increase proportionally, there is only a slow increase of y with l_h (eq. [2.10]), and an increase of the amplitude of the nonthermal power law according to equation (2.13). The appearance of a soft excess power law will depend on the specific values of l_s and l_h . Some illustrative examples of this and the other types of behavior discussed are presented below in § 3.

3. SOFT X-RAY EXCESSES IN THE REFLECTION MODEL

In this section, we will present numerical examples illustrating the results of § 2 in the context of what currently appears to be the pair model with the best chance of meeting observational constraints. The model is essentially that of Z90, which is distinguished from previous models by the inclusion of a component made up of the intrinsic pair plasma radiation Compton-reflected off some nearby distribution of cold matter. The motivation for this type of model stems from the growing body of evidence that the AGN hard X-ray spectra contain a large contribution from reflection of a nonthermal power law off cold matter and are not consistent with single power laws (Pounds et al. 1990; Nandra, Pounds, & Steward 1990;

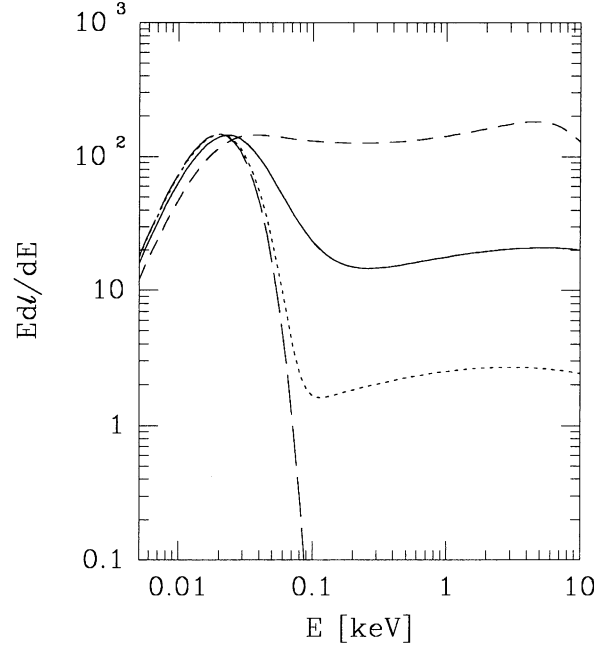


FIG. 4.—Spectra computed in the same manner as for Fig. 1 but with input parameters $l_s = 200$ and $l_h = 40$ (dotted curve; $y \ll 1$, negligible thermal Comptonization), $l_h = 200$ (solid curve; prominent soft excess), $l_h = 1000$ (short dashed curve; significant thermal Comptonization, the amplified nonthermal power law dominates). The long dashed curve shows the un-Comptonized input blackbody spectrum (with temperature $\Theta_s = 10^{-5}$).

Matsuoka et al. 1990; Piro, Yamauchi, & Matsuoka 1990; Turner et al. 1990; Pounds 1990).

Z90 have found that in order for the composite spectrum to have the average 2–20 keV index of $\alpha \sim 0.7$ and the γ -ray spectrum not to exceed the constraint imposed by the cosmic γ -ray background (e.g., Bignami et al. 1979) the hard compactness of the nonthermal pair source must be in the range $30 \lesssim l_h \lesssim 300$. This finding has resolved previous difficulties with the pair cascade model, in which the requirement of $\alpha \sim 0.7$ lead to a γ -ray excess above the constraint from the γ -ray background (Bignami et al. 1979). In the sample calculations presented here, we will therefore also restrict ourselves to this range of l_h . We find that this constraint on l_h combined with the constraints on l_s/l_h and T_s given below by equations (3.1)–(3.2) define a subset in the parameter space that largely coincides with that given in § 2.2 in which we expect to find an observable soft excess. (The reflected component does not directly affect the soft excesses, as a Compton-reflected spectrum appears only above a few keV, see Lightman & White 1988. Hence the discussion presented above in § 2 goes through unchanged.) This explains the occurrence of pronounced soft X-ray excesses in the spectra shown in Z90. Compton reflection models of the type described in Z90 therefore seem to predict that a steep power-law, soft X-ray excess should appear in the spectra of average AGNs.

We will consider here an idealized geometry with a compact nonthermal source of radius R located close above the surface of a slab (possibly an accretion disk), as shown in Figure 5. The power L_h is supplied to e^+e^- pairs in the nonthermal source and radiated as X-rays and γ -rays. One-half of L_h is intercepted by the slab, i.e., the covering factor of the nonthermal source by the slab is 0.5. This and the assumption made below that

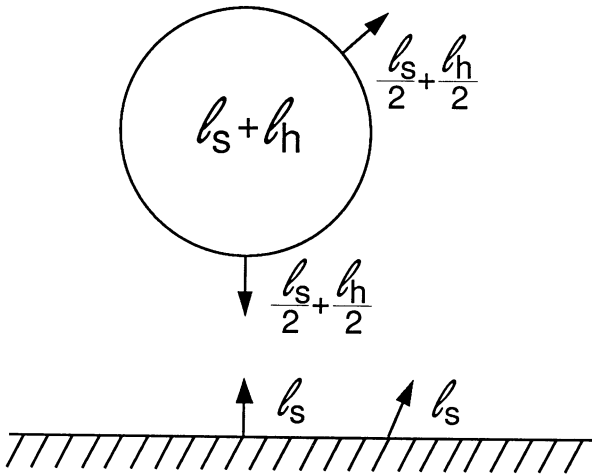


FIG. 5.—A schematic representation of the source region used in the reflection model of § 3.

the covering factor of the hot area of the slab by the source is also 0.5 are motivated by the observations of a short lag time between variations of the fluorescence iron $K\alpha$ line in the X-ray–reflected spectrum and the incident continuum (Kunieda et al. 1990). This suggests that the nonthermal source is in close proximity to the cold matter, and that the area of the cold matter that reprocesses the nonthermal radiation is comparable to the area of the nonthermal source.

Of the $L_h/2$ of luminosity that is hitting the slab, a small fraction $a \approx 0.1\text{--}0.15 \ll 1$ (typical values for the integrated albedo) is Compton-reflected by the slab (White, Lightman, & Zdziarski 1988; Lightman & White 1988; Z90). The remainder is absorbed and reemitted in the form of blackbody radiation. This contributes to the total thermal luminosity of the slab, some of which will be re-intercepted by the pair plasma. The cold matter thus provides a means of self-consistently generating soft photons. As noted, we assume here that the covering factor of the irradiated part of the slab by the nonthermal source is also 0.5. Then, the blackbody luminosity of the irradiated area equals $2L_s$, as L_s is defined as the soft photon luminosity incident on the nonthermal source. The luminosity L_s is isotropically re-emitted by the nonthermal source, and one-half of it returns to the slab. Thus, from energy balance (and using $a \ll 1$),

$$l_s/l_h \gtrsim \frac{1}{3} . \tag{3.1a}$$

where the equality corresponds to no energy generation intrinsic to the disk. Thermal energy may, of course, be internally generated in the slab and radiated (as is the case, e.g., in an accretion disk). If there is equipartition between this internal energy generation and the input of energy to the pair plasma in the form of energetic pairs (as assumed in Z90), energy balance gives,

$$l_s/l_h \simeq 1 . \tag{3.1b}$$

Here we will allow the internal energy generation (and hence L_s) to be varied as a free parameter.

The total luminosity radiated away by both the nonthermal source and the slab equals roughly $(L_s + L_h)/2 + aL_h/2 + L_s$. The three terms here correspond to the direct emission of the nonthermal source, to Compton reflection, and to the part of the thermal emission of the slab that is not intercepted by the nonthermal source, respectively. We neglect here the effects of the reflected radiation $aL_h/2$ returning to the nonthermal source.

The slab blackbody luminosity $2L_s$ is emitted by an area somewhat larger than the projection of the nonthermal source onto the slab, depending on the distance between the slab and the nonthermal source. Taking to this area to be $2\pi R^2$, the blackbody temperature of the region is then

$$kT_s \approx 10 \left(\frac{l_s}{10^2} \right)^{1/4} \left(\frac{R}{10^{14} \text{ cm}} \right)^{-1/4} \text{ eV} . \tag{3.2}$$

For the parameters of $l_h \sim 100$ and $l_s \sim l_h$, found to be typical in the nonthermal model of Z90, $kT_s \sim 10$ eV. Comparing these parameters with the results of § 2, we see that the nonthermal reflection model implies the presence of soft excesses. To illustrate this, we have plotted in Figure 6 the regions of parameter space where an excess is visible for $E_* = 300$ eV and for T_s given by equation (3.2). The plot is constructed in the same manner as Figure 2 except that now T_s varies and is a function of $l_h, l_s/l_h$, and R . The curves shown are for R fixed at the values 10^{13} cm (solid curves) and 10^{14} cm (dotted curves). As in Figure 2, the regions of visible excesses are those enclosed by the curves. Compared to those in Figure 2, the regions are elongated in the l_s/l_h direction since the effect of having a larger l_s/l_h

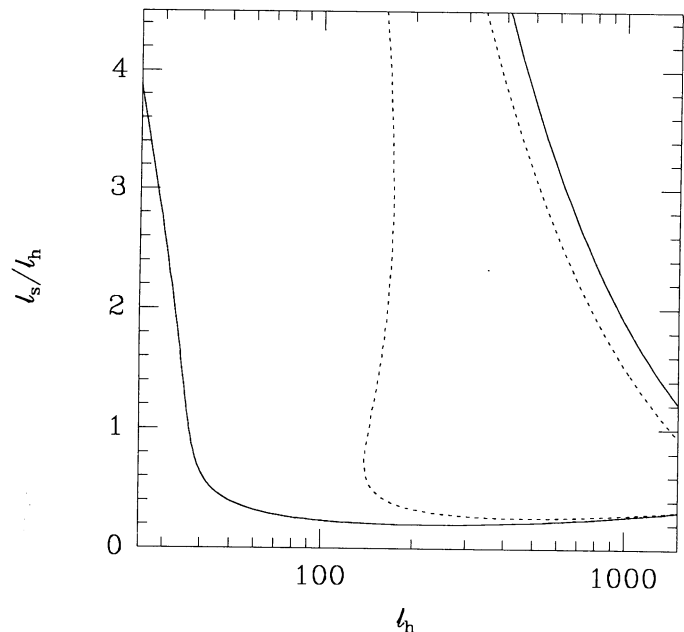


FIG. 6.—The model parameter range $l_h - l_s/l_h$ for which soft X-ray excesses appear in models where the blackbody temperature is a function of the UV luminosity, l_s (see eq. [3.2]). This is the case, in particular, for the reflection model of Z90. Excesses are visible in the region enclosed by the curves. The solid curve is for fixed source size of the nonthermal source of $R = 10^{13}$ cm, while the dotted curve is for $R = 10^{14}$.

and hence a lower Compton temperature is offset by the effect of having a larger l_s and hence a higher blackbody temperature T_s . As can be seen, there is a large range of parameter space over which excesses appear. There is also a strong dependence on R . Excesses become visible for an increasing range of l_h as R decreases. As $L \propto R$ for a fixed Eddington ratio, low-luminosity AGNs should on average show soft excesses more often than high luminosity ones (cf. § 2.2).

The dependence shown in Figure 6 will be modified if the UV bump is not a blackbody. If, e.g., its high-energy end falls off slower than exponentially, soft excesses will appear in a larger range of compactnesses, l_h , than those shown in Figure 6.

We have performed steady state pair cascade calculations as described in LZ87 and ZCL90, with the compactnesses l_s and l_h , the blackbody temperature T_s given by equation (3.2), and monoenergetic pairs injected at $\gamma_{\max} = 2 \times 10^3$ (the X-ray spectra are weakly dependent on the choice of γ_{\max}). We have compared the results with those of the time-dependent code of Coppi (1991) and Coppi & Blandford (1990). We found that if l_s and l_h are changed on time scales $\gtrsim 2R/c$, then the time evolution of the pair source follows approximately a sequence of steady states, for the range of $l_h \leq 300$ considered here. To describe the response of the spectra it therefore suffices to present only the steady state spectra for the initial and asymptotic final states. For example, if a comparison of the initial and final states showed that the hard X-rays softened, an examination of the corresponding time sequence would show a steadily (monotonically) softening hard X-ray spectrum.

Using these steady state spectra, the spectra reflected from the slab were then calculated using the method of Lightman & White (1988), White et al. (1988), and the cosmic abundances of Morrison & McCammon (1983) (see analogous calculations in Z90). The final composite spectra presented below were then constructed by adding the direct pair radiation, the reflected component, and the thermal emission of the slab, as discussed above. We remark that our method is not entirely self-consistent as (1) the slab was assumed to be cold, i.e., its ionization state was not self-consistently calculated taking into account the incoming flux of hard radiation, and (2) the pair

equilibria were found neglecting the presence of reflected radiation.

As pointed out in Z90, addition of the reflected spectra hardens the composite spectra. For $30 \lesssim l_h \lesssim 300$, the 2–20 keV spectral indices of the composite spectra are then $0.6 \lesssim \alpha \lesssim 0.85$, in good agreement with AGN observations. A further consequence of this hardening of the spectrum from the underlying $\alpha \sim 1$ to $\alpha \sim 0.7$ is to enhance the amount of the perceived soft excess (determined by subtracting off from the observed flux a power law extrapolated from the 2–20 keV range). Decomposition of total spectra into the direct and the reflected components is given in Z90. The various features that appear in the direct pair spectra have been extensively discussed elsewhere, e.g., in LZ87, and will not be reanalyzed here.

We present in Figure 7 some representative examples of the composite spectra we computed. Depending on the variability pattern of the input l_h and l_s , we can observe distinct variability patterns of the soft and hard X-rays. The spectra presented illustrate two possible types of variability which correspond to some of the characteristic AGN variability patterns discussed in § 1.

1. Variable l_s , constant l_h . Figure 7a shows two spectra for $l_h = 300$ and varying $l_s = 100, 300$. It can be seen that the spectrum above 1 keV preserves its shape, while dramatic variations occur in the spectrum and flux below ~ 0.5 keV (see Table 1). This is because the underlying hard X-ray power law is due mostly to blackbody photons Compton upscattered by the nonthermal pair distribution, which for $l_h \gtrsim l_s$ is independent of the blackbody temperature and luminosity (Zdziarski & Lightman 1985). For $l_h \lesssim l_s$, the hard flux becomes anticorrelated with the soft flux. This is due to the effect of upscattering by the thermalized pairs of the nonthermal power law, which is an effect increasing with increasing l_h and decreasing l_s (see eq. [2.13] and § 2.1).

2. Proportional variations of the power released in both the nonthermal source and the disk. If the power released in the slab equals xL_h , then energy balance gives

$$\frac{l_s}{l_h} \simeq \frac{2}{3}x + \frac{1}{3}. \quad (3.3)$$

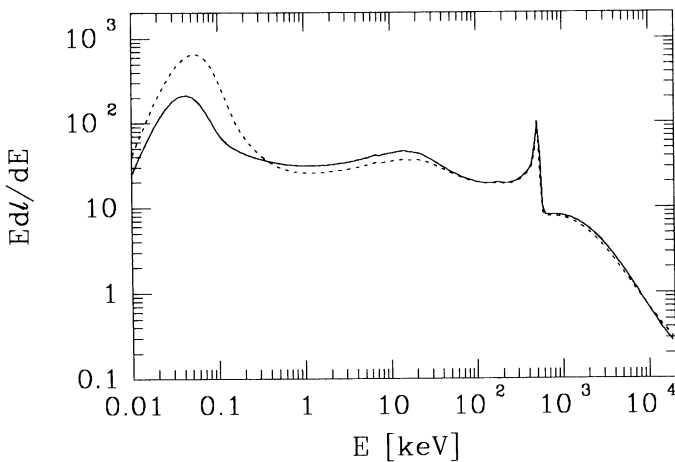


FIG. 7a

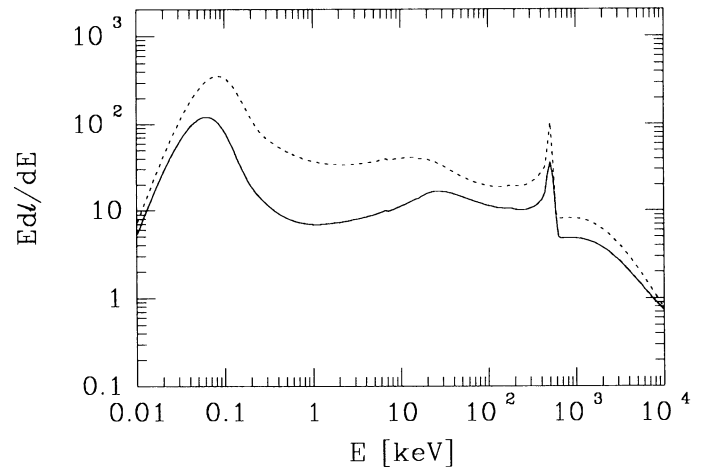


FIG. 7b

FIG. 7.—Composite spectra from pair cascade sources located above a slab of cold material. The parameters of different models are given in Table 1. The solid and dotted curves in Figs. 7a and 7b correspond to models a1, 2 and b1, 2 in Table 1, respectively. See § 3 for discussion. The $K\alpha$ iron line at 6.4 keV is not included. The spectra shown are for angle-averaged emission of both the nonthermal source and the slab, and their normalization corresponds to emission from the both sides of the slab (e.g., an accretion disk).

TABLE 1
PARAMETERS AND RESULTS FOR THE PRESENTED MODELS

l_h	l_s	kT_s (eV)	kT_c (keV)	τ_T	a	$l_{0.1-1 \text{ keV}}$	$l_{2-20 \text{ keV}}$	$\alpha_{2-20 \text{ keV}}$	Model
300.....	100	10	2.4	7.6	0.12	95	92	0.82	a1
300.....	300	13	1.3	7.1	0.11	170	74	0.84	a2
100.....	56	15	4.2	4.0	0.16	46	24	0.67	b1
300.....	267	20	1.9	7.7	0.11	250	87	0.90	b2

NOTES.— $\gamma_{\text{max}} = 2000$ for all models; $R = 10^{14}$ cm and 10^{13} cm in models a and b, respectively.

Figure 7b shows the case with $l_h = 100, 300$ and $x = \frac{1}{3}$. In that case, both the soft and hard X-ray fluxes are approximately correlated, with the hard X-ray spectra softening with increasing compactness, which is a general feature of pair models (e.g., S87; LZ87). The energies to which the soft X-ray excesses extend increase with the compactness.

4. DISCUSSION AND CONCLUSIONS

Most current explanations of the hard X-ray spectrum in AGNs rely on the existence of a pair plasma in their interiors. In this mechanism, energetic pairs upscatter soft photons to X-ray energies, quickly losing most of their energy in the process. From both simple order-of-magnitude estimates based on observed X-ray luminosities and variability time scales (e.g., Guilbert et al. 1983) and the results from pair plasma models, one finds that enough of these cooled pairs accumulate to form a Thomson thick thermal plasma. This plasma can have significant effects on the observed source spectrum. As shown in this work, this thermal plasma is likely to produce an excess of emission at $\lesssim 1$ keV on top of the pre-existing hard X-ray power law. This will complement any other source of soft X-ray emission one might envision such as the inner edge of an accretion disk. In this regard, we note that a cloud of hot pairs plays a role identical to (and may be precisely) the hot corona referred to in some accretion disk models (e.g., Czerny & Elvis 1987; Czerny & Zbyszewska 1991) as a way of extending disk emission and producing a soft excess. In pair plasma models, however, the density and temperature of the hot corona are not free parameters but rather are determined self-consistently.

One possible argument against having the soft excess comes from the same source as the hard X-rays is that the two components often show largely uncorrelated time variability. When a pair plasma is involved, however, different energy bands may respond in different manners to changes in the pair plasma inputs (e.g., see Coppi 1991). As shown above, the soft excess versus hard X-ray behavior is such a case. It appears possible to construct scenarios that reproduce a variety of variability behavior, e.g., variable soft X-rays and constant hard X-rays as well as overall correlation between soft and hard X-rays; see §§ 2.3 and 3. A general prediction of the present model is that the soft X-rays should vary on time scales comparable to those seen in the hard X-rays. (The amplitudes of variation need not be similar, however.) If the soft X-rays are not seen to vary, an additional and dominant source of soft X-ray emission, e.g., from a much larger region, must be invoked. This may well be the case in some sources (see, e.g., NGC 4151 observations by Pounds et al. 1986b).

Another test for or constraint on pair plasma-based models of the soft excess comes from the detailed shape and amplitude of the excess (see §§ 2 and 3). Again, however, current observations are not of high enough quality to address this issue. (*ROSAT* and *BBXRT* may soon change this situation, however.) The excesses produced in pair plasma-based models are steep featureless power laws, and any features in the underlying un-Comptonized UV distribution would tend to be smeared out by the Comptonization. Observation of a significantly non-power-law excess, e.g., one with absorption features that vary with the soft X-ray continuum, would probably rule out the simple pair plasma explanation of that soft excess, requiring, e.g., the presence of additional intervening matter.

We predict that provided the nonthermal reflection model discussed in § 3 proves to be qualitatively correct, soft excesses should be common in AGNs. This is due to the approximate coincidence of the parameter space determined for the nonthermal reflection model with the parameter space required for the appearance of soft X-ray excesses; see § 3. This is to be contrasted with the accretion disk picture where current models (without hot coronae) typically need to be viewed almost face-on to give excess spectra extending to sufficiently high energies, i.e., where soft excesses would be relatively rare.

Our model predicts two main correlations of soft X-ray excesses with AGN parameters. First, the frequency of occurrence of soft X-ray excesses is expected to be larger in objects with steeper hard X-ray slopes, which thus have larger hard compactnesses (see § 2). Second, in any model in which the origin of the seed UV photons is thermal (e.g., the reflection model), there should be also a strong correlation between the size of the UV-emitting region (and hence its temperature; see eq. [3.2]) and the maximum energy at which an excess is visible. For a given Eddington ratio, soft excesses should be seen more often in low-luminosity AGNs, which are likely to have smaller central engines. As the range of the Eddington ratio inferred observationally seems to span only one or two orders of magnitude (e.g. Padovani 1989) as compared to the range of AGN luminosities spanning seven or so orders of magnitude, there should also be the same overall correlation with L for all AGNs.

The authors acknowledge valuable comments on this work by Roger Blandford and Roland Svensson. One of us (P. S. C.) has been supported in part by NASA grants NAGW-830, NAGW-1636, and NAGW-1301, NSF grants AST 86-15325 and AST 89-15326, and the STScI collaborative visitor program.

REFERENCES

- Arnaud, K. A., et al. 1985, *MNRAS*, 217, 105
 Begelman, M. 1990, talk delivered at the Workshop on Variability of Active Galactic Nuclei, Atlanta
 Bignami, C. F., Fichtel, C. E., Hartman, R. C., & Thomson, D. J. 1979, *ApJ*, 232, 649
 Coppi, P. S. 1991, *MNRAS*, in press

- Coppi, P. S., & Blandford, R. D. 1990, MNRAS, 245, 453
 Czerny, B., & Elvis, M. 1987, ApJ, 321, 305
 Czerny, B., & Zbyszewska, M. 1991, MNRAS, in press
 Done, C., Ghisellini, G., & Fabian, A. C. 1990, MNRAS, 245, 1
 Elvis, M., Green, R. F., Bechtold, J., Schmidt, M., Neugebauer, G., Soifer, B. T., Matthews, K., & Fabbiano, G. 1986, ApJ, 310, 291
 Elvis, M., Wilkes, B. J., & Tananbaum, H. 1985, ApJ, 292, 357
 Fabian, A. C., Blandford, R. D., Guilbert, P. W., Phinney, E. S., & Cuellar, L. 1986, MNRAS, 221, 931
 Ghisellini, G., Done, C., & Fabian, A. C. 1989, in 23rd ESLAB Symposium, ed. J. Hunt & B. Batrick (ESA SP-296) (Noordwijk: ESA), 789
 Guilbert, P., Fabian, A. C., & Rees, M. J. 1983, MNRAS, 205, 593
 Halpern, J. P. 1984, ApJ, 281, 90
 Krolik, J. H., McKee, C. F., & Tarter, C. B. 1981, ApJ, 249, 422
 Kunieda, H., Turner, T. J., Awaki, H., Koyama, K., Mushotzky, R. F., & Tsusaka, Y. 1990, Nature, 345, 786
 Lightman, A. P., & White, T. R. 1988, ApJ, 335, 57
 Lightman, A. P., & Zdziarski, A. A. 1987, ApJ, 319, 643 (LZ87)
 Maraschi, L., Chiapetti, L., Falomo, R., Garilli, B., Malkan, M., Tagliaferri, G., Tanzi, E. G., & Treves, A. 1991, ApJ, 368, 138
 Matsuoka, M., Piro, L., Yamauchi, M., & Murakami, T. 1990, ApJ, 361, 440
 Morrison, R., & McCammon, D. 1983, ApJ, 270, 119
 Nandra, K., Pounds, K. A., & Stewart, G. C. 1990, MNRAS, 242, 660
 Padovani, P. 1989, A&A, 209, 27
 Pan, H. C., Stewart, G. C., & Pounds, K. A. 1990, MNRAS, 242, 177
 Piro, L., Massaro, E., Perola, G. C., & Molteni, D. 1988, ApJ, 325, L25
 Piro, L., Yamauchi, M., & Matsuoka, M. 1990, ApJ, 360, L35
 Pounds, K. A. 1990, MNRAS, 242, 20P
 Pounds, K. A., Nandra, K., Stewart, G. C., George, I. M., & Fabian, A. C. 1990, Nature, 344, 132
 Pounds, K. A., Turner, T. J., & Warwick, R. S. 1986a, MNRAS, 221, 7P
 Pounds, K. A., Warwick, R. S., Culhane, J. L., & de Korte, P. A. J. 1986b, MNRAS, 218, 685
 Rothschild, R. E., Mushotzky, R. F., Baity, W. A., Gruber, D. E., Matteson, J. L., & Peterson, L. E. 1983, ApJ, 269, 423
 Rybicki, G. R., & Lightman, A. P. 1979, Radiative Processes in Astrophysics (New York: McGraw-Hill)
 Shapiro, S. L., Lightman, A. P., & Eardley, D. M. 1976, ApJ, 204, 187
 Sunyaev, R. A., & Titarchuk, L. G. 1980, A&A, 86, 121 (ST80)
 Svensson, R. 1987, MNRAS, 227, 403 (S87)
 Turner, M. J. L., et al. 1990, MNRAS, 244, 310
 Turner, T. J., & Pounds, K. A. 1988, MNRAS, 232, 463
 ———. 1989, MNRAS, 240, 833
 Urry, C. M., Arnaud, K., Edelson, R. A., Kruper, J. S., & Mushotzky, R. F. 1989, in 23rd ESLAB Symposium, ed. J. Hunt & B. Batrick (ESA SP-296) (Noordwijk: ESA), 695
 Warwick, R. S., Barstow, M. A., & Yaqoob, T. 1989, MNRAS, 238, 917
 White, T. R., Lightman, A. P., & Zdziarski, A. A. 1988, ApJ, 331, 939
 Wilkes, B. J., & Elvis, M. 1987, ApJ, 323, 243
 Yaqoob, T., Warwick, R. S., & Pounds, K. A. 1989, MNRAS, 236, 153
 Zdziarski, A. A., Coppi, P. S., & Lamb, D. Q. 1990a, ApJ, 357, 149 (ZCL90)
 Zdziarski, A. A., Ghisellini, G., George, I. M., Svensson, R., Fabian, A. C., & Done, C. 1990b, ApJ, 363, L1 (Z90)
 Zdziarski, A. A., & Lightman, A. P. 1985, ApJ, 294, L79